ISSN 1070-3632, Russian Journal of General Chemistry, 2008, Vol. 78, No. 4, pp. 833–845. © Pleiades Publishing, Ltd., 2008.
Original Russian Text © A.A. Levin, S.P. Dolin, T.Yu. Mikhailova, 2007, published in Rossiiskii Khimicheskii Zhurnal, 2007, Vol. 51, No. 5, pp. 139–148.

Quantum Chemistry of Hydrogen-bonded Materials. Ferroelectrics and Antiferroelectrics

A. A. Levin, S. P. Dolin, and T. Yu. Mikhailova

Kurnakov Institute of General and Inorganic Chemistry, Russian Academy of Sciences,
Lebinskii pr. 31 119991, Moscow, Russia
tel: (495)9554850
e-mail: levin@ igic.ras.ru

Received July 26, 2007

Abstract—Some aspects of application of quantum chemical approaches and methods in the microscopic theory of hydrogen-bonded ferroelectrics and antiferroelectrics, as well as their deuterated analogs, were reviewed in the context of original works of the authors. Calculations of the spontaneous polarization of KH_2PO_4 (KDP) and charge transfer "channels" in transition of KDP and other H-bonded crystals from paraphase to an ordered phase were discussed, as well as the factors responsible for difference in the ferroactive behavior between KDP and $NH_4H_2PO_4$ (ADP). In terms of the dynamic Ising model and in the mean field approximation, the potentialities of quantum chemical approaches were analyzed as applied to examination and prediction of the results of order-disorder structural phase transitions in $M_3H(AO_4)_2$ family materials, 5X derivatives of 9-hydroxyphenalenone, and crystalline chromous acid α-$HCrO_2$ in relation to deuteration of the H-bonds in these crystals.

DOI: 10.1134/S1070363208030427

This study is dedicated to a new direction in quantum chemistry of solid state, application of quantum chemical approaches and computational methods in studying hydrogen-bonded materials. The latter are of interest not only for fundamental science, but also as candidate ferroelectrics [1], nonlinear optics crystals [2], and superprotonic conductors [3], promising, in particular, for hydrogen fuel cell applications [4, 5].

We discuss here ferroelectrics and antiferroelectrics with intermolecular and intramolecular symmetric strong hydrogen bonds, as well as their deuterated analogs. We focused on those properties of the H/D-bonded crystals, that allow classifying them as specific functional materials. The systematic development of quantum chemistry of such materials, to which we significantly contributed with our studies, is in its early stage, for which reason this review is inevitably fragmentary and based on the results of those studies.

H/D-Bonded Ferroelectrics and Antiferroelectrics

A preliminary idea of the ferroelectric and antiferroelectric materials we discuss here is given by Figure 1 demonstrating the structure of the best known among them, potassium dihydrophosphate KH_2PO_4 (abbr. KDP), a typical representative of the family with the general composition $M(H/D)_2AO_4$, where M = K,

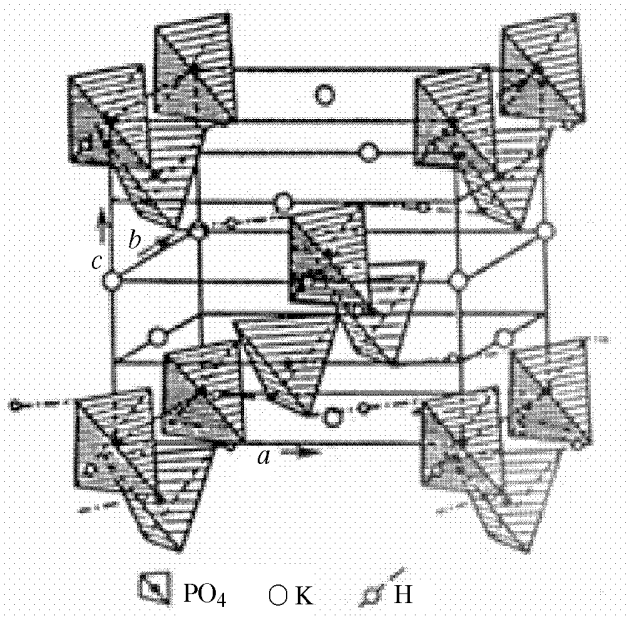

Fig. 1. Crystal structure of KH_2PO_4.

Rb, Cs and A = P or As [1, 6]. Each of the linear symmetric hydrogen bonds with a length of ~2.50 Å, interconnecting in the KDP crystal the neighboring PO_4 tetrahedrons, can occur in two equivalent states, O–H···O or O···H–O. They correspond to two possible equilibrium proton positions that differ by 0.36 Å.

At atmospheric pressure and temperatures above the critical point (T_c = 123 K) all the protons in the crystal are randomly distributed over these two positions. At T_c, KDP exhibits a structural phase transition from the disordered paraelectric phase (paraphase) of the crystal to a proton-ordered low-temperature ferroelectric phase. In the latter, two out of the four hydrogen atoms nearest to each PO_4 tetrahedron, e.g., the "bottom" hydrogen atoms, are characterized by short distances of 1.07α corresponding to covalent O–H bonds, and the two "top" H atoms, by long distances of 1.43 Å, corresponding to O···H hydrogen bonds. Also possible is the opposite situation, when two kinds of the H atoms change roles.

Evidently, such ordering of the H atoms and their nuclei, protons, is responsible for emergence in the ferroelectric phase of both local dipole moments in each individual structural unit and of macroscopic spontaneous polarization P_s of the crystal along axis *z*, persisting in the absence of an external electric field.

A compound with a slightly different composition, ammonium dihydrophosphate $NH_4H_2PO_4$, at a temperature lower than another critical point (148 K) exhibits a transition of the paraphase to a low-temperature antiferroelectric phase. In the latter phase, ordering of protons of the H-bonds is also responsible for emergence of local dipole moments, but the local moments of different structural units are parallel to the xy plane and compensate one another, thereby precluding the macroscopic polarization of the sample. The collective transfer of protons along the H-bonds (by tenth fractions of angstrom) in the case of the ferro- or antiferroelectric ordering of the proton subsystem is accompanied by less significant displacements of the P atoms and K^+ cations, or P atoms and NH_4^+ ions (by hundredth fractions of angstrom). A more or less similar behavior is also typical for other H/D-bonded ferro- and antiferroelectrics, some of which are discussed below.

Charge Distribution and Spontaneous Polarization

The spontaneous polarization of the KH_2PO_4 crystal was theoretically estimated for the first time as early as 1950–1960s [6] in terms of the ionic crystal model that gained wide acceptance in those years. Calculation of the spontaneous polarization P_s of the H-bonded ferroelectric, based on the modern concepts of quantum chemistry, was attempted much more recently. Initially, the charge distribution and P_s in KDP were calculated [7, 8] for a model bitetrahedral cluster $[(HO)_3PO–H\cdots OP(OH)_3]^+$ (Fig. 2a), taken as an example; this is an idealized representation of a similar fragment from the structure of the crystal. The P–O, O–H, and O···H distances were taken from the diffraction data. Calculations by the Hartree-Fock method (RHF) were carried out in the STO-3G basis for the occupied AOs of phosphorus and oxygen and for 1s AO of hydrogen. Also, we used the semi-empirical MNDO/H scheme specially intended for description of H-bonded systems [9]. In the latter case, the negative Mulliken charges of hydrogen- and covalently-bonded atoms, $O_{O\cdots H}$ and $O_{O–H}$, differ by ca. –0.2, and the positive charge of the bridging H atoms is ca. 0.35. As a result, the dipole moment μ_α for the $[H_2PO_4]^-$ anion in the ferroelectric phase of the KH_2PO_4 crystal was estimated at –4.8 D, which is fairly close to μ_α = –6.3 D estimated from the experimental spontaneous polarization of the KH_2PO_4 crystal [10]. Both these values refer to the case when the center of the PO_4 tetrahedron was chosen as the coordinate origin.

For comparison, we carried out MNDO/H calculations for the pentatetrahedral cluster $[H_{16}(PO_4)_5]^+$ (Fig. 2b) with four bridging and twelve terminal hydrogen atoms, in which the central PO_4 tetrahedron is surrounded by four tetrahedrons of the same kind, like in the real KH_2PO_4 crystal. Based on the charge distribution for the central PO_4 tetrahedron and the bridging H atoms, similar to that obtained earlier, we estimated μ_α at –4.1 D. It should also be noted that, in this case, like in the case of the bitetrahedral cluster, the optimized position of the phosphorus atom in the central tetrahedron fairly closely corresponds to the displacement of the P atom from $O_{O–H}$ toward $O_{O\cdots H}$ atoms, experimentally observed in the ferroelectric phase of the KH_2PO_4 crystal. The calculation yielded shortening of the $P–O_{O\cdots H}$ bond by 0.02 Å, which is nearly identical to 0.02–0.03 Å derived from the experiment [11].

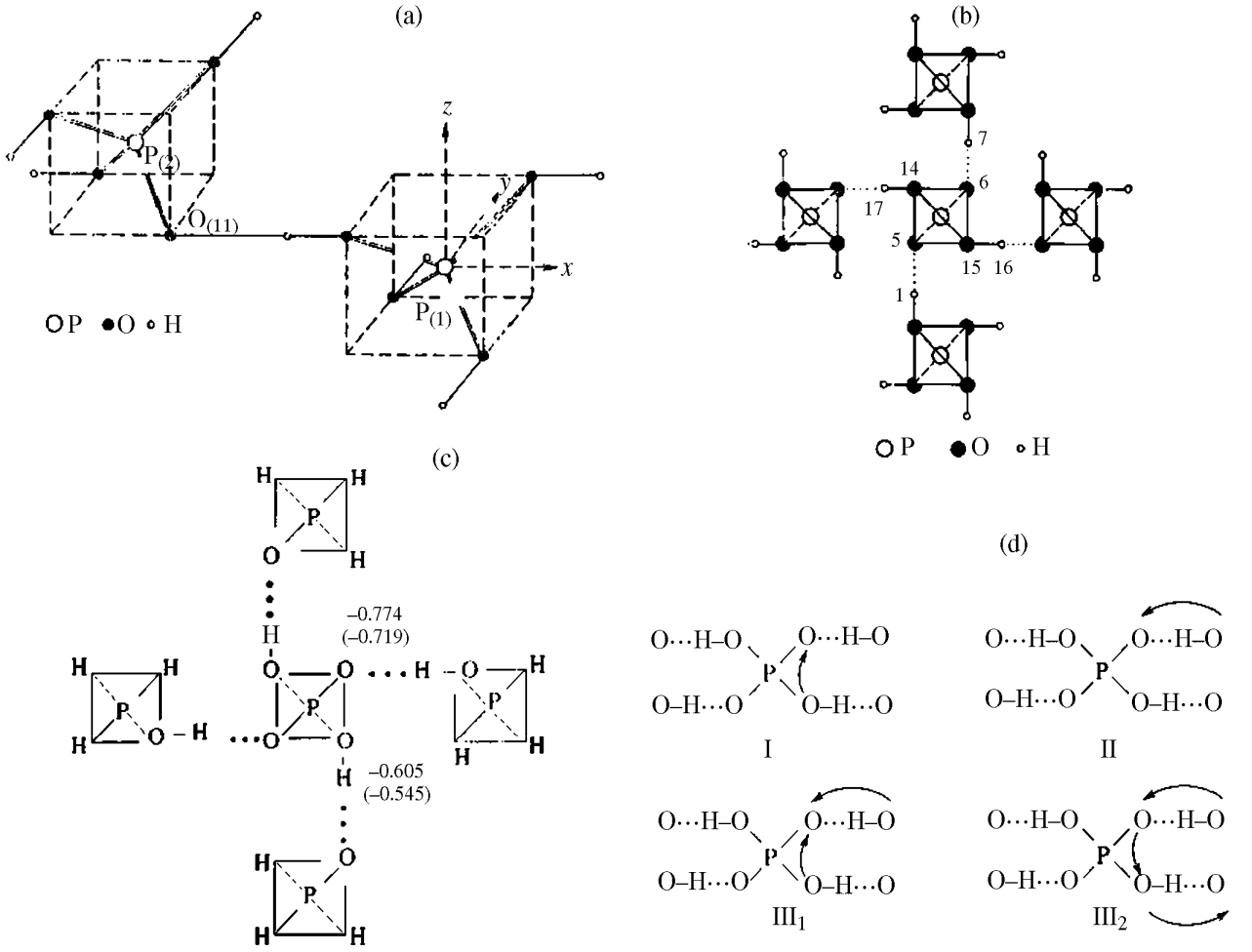

Fig. 2. (a–c) Charge distribution calculations for (a) bitetrahedral cluster, (b) pentatetrahedral cluster, (c) simplified pentatetrahedral cluster [the figures are the effective charges on the O atoms, calculated using canonical MOs (not parenthesized) and localized MOs (parenthesized)] and (d) charge transfer channels: (I) intramolecular transfer, (II) intermolecular transfer, and (III_1 and III_2) resultant transfer in the KH_2PO_4 crystal.

Charge Transfer Channels

The atomic charges describe the charge redistribution in the crystal, associated with proton ordering, in insufficient detail, as they do not provide information about the occupancies of individual AOs involved in interatomic bonding. We determined these parameters for the KH_2PO_4 crystal [12, 13] using Boys transformation [14] of the occupied canonical MOs to localized MOs in the $[H_4PO_4{\cdot}4OPH_3]^+$ model pentatetrahedral cluster (see Fig. 2c), in which, compared to the cluster in Fig. 2b, the terminal P–OH bonds are replaced by the P–H bonds. Among the localized MOs, we identified with reasonable accuracy the (hybrid) AOs, either participating in chemical bonding or corresponding to unshared electron pairs. Comparison of the occupancies for these AOs clearly demonstrates the routes (channels) for electron charge transfer associated with changing positions by protons of the H-bonds and reveals somewhat unexpected character of the charge transfer.

It could be presumed a priori that, e.g., the ferroelectric proton ordering will entail transfer of the excess electron density to each $O_{O\cdots H}$ atom mainly from the O_{O-H} atoms of the same PO_4 tetrahedron (the intramolecular mechanism, Fig. 2d, I). An alternative consists in the intermolecular transfer mechanism (II); also possible are mixed mechanisms (III_1 or III_2). In reality, it turned out that the excess electron density on the $O_{O\cdots H}$ atoms is due mainly to intermolecular transfer to each of them of ca 0.2 units of negative

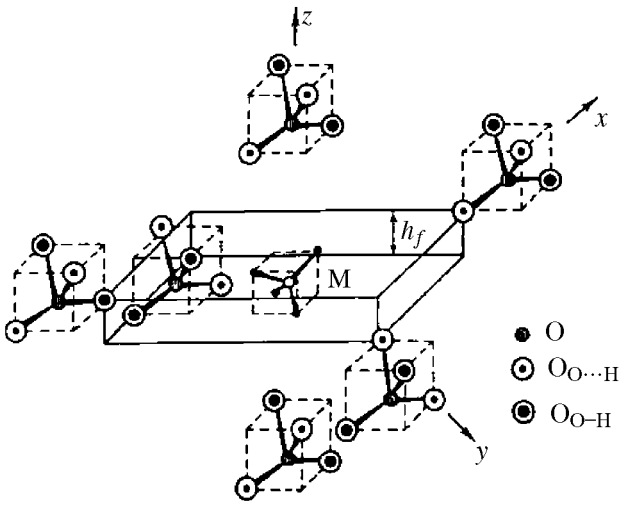

Fig. 3. Nearest surrounding of the M^+ cation in MH_2PO_4 crystals: cluster I.

charge from the O_{O-H} atoms of the neighboring PO_4 tetrahedrons. This transfer is compensated in part (Fig. 2d, III_2) by the reverse transfer of ca. 0.1 units of negative charge via intramolecular channels, which yields the resultant charge difference of nearly 0.2 electrons between the $O_{O\cdots H}$ and O_{O-H} atoms of the crystal and the above-mentioned electronic contribution to μ_α and P_s.

In other words, the O_{O-H} atoms act as intermolecular donors and intramolecular acceptors of electron density, while the $O_{O\cdots H}$ atoms, on the contrary, as intramolecular electron donors and intermolecular electron acceptors. This suggests a similarity between the stereochemistry of the AO_4 tetrahedrons in materials from the KDP family and the geometry of heterolinand molecules AL_2X_2, like CH_2F_2, $PH_2F_2^+$, etc. [15]. The latter exhibit shortening of the A–donor and lengthening of the A–acceptor bonds in comparison with the initial homoligand systems, attributed, in terms of the second-order perturbation theory, to the change of the adiabatic potential of the homoligand system, associated with the ligand substitution [16, 17]. A similar phenomenon is observed in ferroelectrics of the KDP type. In the paraphase–ferroelectric phase transition, the phosphorus atom in each of the AO_4 tetrahedrons is displaced from the center to the $O_{O\cdots H}$ atoms from the O_{O-H} atoms, which causes changes in the corresponding A–O bond lengths.

Similar analysis of the occupancies of the localized AOs for an organic crystal layer of squaric acid $H_2C_4O_4$ and the molecular chain in 1,3-cyclohexanedione crystal, containing conjugated bonds, shows that the relationships revealed for KH_2PO_4 crystal are valid for these systems as well. However, the intermolecular charge transfer occurs mainly via σ bonds, and the intramolecular transfer primarily involves the $p\pi$ AOs of carbon and oxygen [13].

Ferroactive Behavior of KH_2PO_4 and $NH_4H_2PO_4$ Crystals

As known, all $M(H/D)_2AO_4$ (M = K, Rb, and Cs) materials belonging to the KDP family are ferroelectrics, and materials with M = NH_4, antiferroelectrics [1], but the physicochemical factors responsible for this difference still remain to be conclusively established. In [18, 19] we studied the behavior of the M^+ cations in the $H_2AO_4^-$ framework, associated with ferro- or antiferroelectric proton ordering for three model clusters with the filled electron shells: $[M(H_2PO_4)_6]_5^-$ (I) shown in Fig. 3, $[M(H_4PO_4)_6]_7^+$ (II) close to (I) in the composition and structure, and $[M(H_4PO_4)_2(H_2PO_4{\cdot}HO{-}PH_3)_4]_3^+$ cluster (III).

The central position in the cluster, M, is occupied by NH_4^+ (displayed) or an alkali-metal ion. Antiferroelectric proton ordering is shown. In ferroelectric ordering, the O–H groups are located on the top, and O^- ions simulating the $O^{\cdots}H$ groups, on the bottom, edge of each tetrahedron from the M^+ cation surrounding.

Clusters I and II simulate the surrounding of M^+ in the first coordination sphere by six PO_4^- tetrahedrons (Fig. 3), and cluster III takes into account also the tetrahedrons from the second coordination sphere of the M^+ cation [19].

We carried out calculations by MNDO and MNDO/H methods, in which the ammonium ions were taken as such, while potassium, rubidium, and cesium cations were replaced by Na^+, Li^+ ions and the point charge q^+ because the semiempirical schemes we used lack the necessary parameters for K, Rb, and Cs. The R_e, R_a distances between the cluster center M and the equatorial and axial oxygen atoms, closest to the center (see Fig. 3) were taken from the diffraction data for the equatorial and axial K–O, N–O interatomic distances in the KH_2PO_4 and $NH_4H_2PO_4$ crystals.

We found that, for "empty" clusters I and II, i.e., those without M^+ cation, the antiferroelectric proton ordering is always energetically more favorable than

the ferroelectric ordering, with the NH_4^+ ion at the center of the cluster providing further stabilization of the system. The calculated potential energy profiles suggest a minor displacement (by hundredth fractions of angstrom) of the ammonium ion from the center of the cluster in the *xy* plane, corresponding to formation of the N–H···O bonds, whose existence was presumed earlier [20, 21].

In the case of cluster III, we used the above-mentioned experimental interatomic N–O distances for R_e, R_a and obtained the results identical to those in the case of clusters I and II. However, the situation is qualitatively different when the R_e, R_a parameters are taken from the data for KH_2PO_4: Ferroelectric proton ordering becomes energetically favorable even in the "empty" cluster. The Na^+ ion at the center of the ferroelectric cluster favors its further stabilization and is displaced preferably along the *z* axis (by 0.01 Å).

Pseudospin Hamiltonian and Molecular Field

The paraphase-ordered phase structural transition is studied in terms of the microscopic theory of hydrogen-bonded materials using the static and dynamic pseudospin Ising models [1, 22]. The static model utilizes the pseudospin Hamiltonian :

$$H = -\frac{1}{2}\sum_{i,j}^{N} J_{ij}\sigma_i\sigma_j. \qquad (1)$$

It describes the total energy of effective two-particle interactions of the protons or deuterons from the H/D bonds in a crystal using the Ising model interaction parameters J_{ij} (from here on, J_{ij} parameters are treated as corresponding to interaction between ith and jth H/D bonds, for brevity).

In this classical (nonquantum) version, σ_i signifies pseudospin variables, each of which takes two values, $\sigma_i = (+1, -1)$, corresponding to the two equilib-rium positions of a proton/deuteron on the *i*th H/D bond: O–H···O or O···H–O.

In the dynamic (quantum) version, the pseudospin Hamiltonian has the following appearance:

$$H = -\Omega\sum_{i,j}^{N}\sigma_i^x - \frac{1}{2}\sum_{i,j}^{N} J_{ij}\sigma_i^z\sigma_j^z. \qquad (2)$$

Here, Ω is the tunneling parameter taking into account the quantum motion of a proton or deuteron along each of the H/D bonds; it is equal approximately to the half of the energy gap Δ_{01} between the ground and first excited vibrational states of the proton/deuteron in the corresponding double-well potential (Fig. 4). The parameters J_{ij} have essentially the same physical meaning as in (1), and σ_i^x, σ_i^z are standard matrices of the Pauli operators, represented in the basis of the wavefunctions of the proton/deuteron localized in individual potential wells of its double-well potential profile on the *i*th H/D bond.

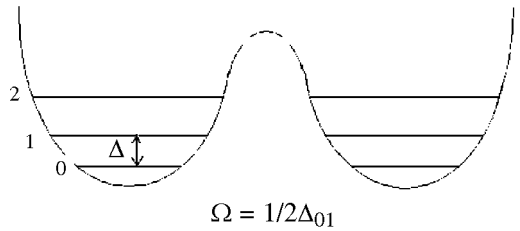

Fig. 4. Potential profile and vibrational levels of a proton/deuteron.

In the elementary mean field theory (the molecular field approximation), the critical temperature T_c of a structural phase transition from a high-temperature (paraelectric) phase to a low-temperature ordered phase is determined by the formula [1, 22]:

$$T_c = (J_0/k_B)(2\Omega/J_0)\{\ln[1+(\Omega/J_0)] - \ln[1-(\Omega/J_0)]\}^{-1}, \qquad (3)$$

where $J_0 = \sum_j J_{ij}$ is the molecular field parameter, and k_B, Boltzmann constant.

Expression (3) yields a simple criterion for the occurrence of a structural phase transition:

$$\text{a transition occurs at } \Omega/J_0 < 1, \qquad (4a)$$

$$\text{no transition occurs at } \Omega/J_0 \geq 1. \qquad (4b)$$

Mechanisms of Formation of Ising Parameters

The conventional theory of H-bonded materials did not calculate the parameters of Hamiltonians (1) and (2); they were found for each specific material by fitting to the values of a number of specially measured physical characteristics (see typical examples in [22–24]). Hence, qualitatively, one of the major tasks of quantum chemistry of such materials consists in elucidating the physicochemical mechanisms of formation of the parameters of Hamiltonians (1) and (2), and quantitatively, in theoretical calculation of these parameters. This is essential for understanding

the relationship between the properties of the materials examined and their chemical composition and structure, as well as for sound molecular designing of such materials. Special attention should be given to Ising parameters, since, by contrast to the precise definition of the parameter Ω, the above-presented definition of the parameters J_{ij} is unsuitable for more specific identification of their formation mechanism and calculation method.

Direct Electrostatic Mechanism

The elementary mechanism of formation of Ising parameters, known since as early as 1963 [25], implies electrostatic interaction of the reversed dipoles arising upon transfer of the charge of protons/deuterons between their equilibrium positions on the H/D bonds. For this mechanism, the parameters J_{ij} can be found by the formula [22]:

$$J_{ij} = \frac{1}{4}[V_{ij}(+, -) + V_{ij}(-, +) - V_{ij}(+, +) + V_{ij}(-, -), \quad (5)$$

where $V_{ij}(\alpha, \beta)$ ($\alpha, \beta = +, -$) is the energy of the Coulomb interaction of two point protons/deuterons occupying their equilibrium positions (α, β) on ith and jth H/D bonds.

This mechanism was regarded as realistic for a fairly long time. However, we pointed out more recently [26] that the calculations of the $V_{ij}(\alpha, \beta)$ parameters should utilize the effective charges of hydrogen atoms, rather than the charges of "bare" protons. The effective charges of the hydrogen atoms were estimated [26] according to Mulliken and Löwdin, via cluster semiempirical (MNDO/H, AM1, PM3) and ab initio (RHF/3-21 and RHF/6-31) calculations for KH_2PO_4 crystals and squaric acid [8], as well as for crystals of the $K_3H(SO_4)_2$ type and their deuterated analogs (TKHS family, see below). Based on the direct electrostatic mechanism, we calculated [26, 27] the Ising parameters for all these materials with different compositions and dimensionalities of the H-bond network. The resulting values were no greater than 10–30 K, which is several times, and in some cases by an order of magnitude, smaller than the corresponding "experimental" values obtained by fitting. Hence, the direct electrostatic mechanism should not always be treated as necessarily adequate.

The Indirect Electrostatic Mechanism and Electrostatic Model

The indirect electrostatic mechanism of formation of Ising parameters should imply the interaction of the reversed dipoles induced by transfer of protons/deuterons in a "nonhydrogen skeleton of the crystal, but the real mechanism always combines the direct and indirect components [26, 27]. Such a combined electrostatic mechanism of formation of Ising parameters seems plausible for materials with zero-dimension (0-D) network of the H/D bonds, e.g., for crystals belonging to the TKHS family, in which the main ferroactive structural units are represented by isolated $[(H/D)(AO_4)_2]_3^-$ dimers. Hence, the J_{ij} parameters can be calculated by formula (5), but the $V_{ij}(\alpha, \beta)$ terms in this formula should be treated as the energies of interaction of the total charge distributions in space of *i*th and *j*th dimers, respectively, for α and β positions of protons/deuterons. Calculation of these distributions and their interaction energies showed that this approach, i.e., the electrostatic model [28, 29], provides realistic values of Ising parameters which reasonably agree with the results of "nonmodel" calculation in terms of the pseudospin cluster method (see below).

Indirect Nonelectrostatic Mechanism

A mechanism absolutely different from the two mechanisms discussed above operates in materials with a nonzero dimensionality of the H-bond network, such as crystals from the KDP family or a squaric acid crystal layer. In such materials, every molecular structural unit is surrounded by hydrogen atoms, to each of which it is either covalently- (O–H) or H-bonded (O···H). A good example can be found in a KH_2PO_4 crystal in which such unit is represented by the PO_4 tetrahedron. Replacement of selected O–H bonds by O···H bonds, as well as the reverse process, are responsible for rearrangement of the electronic structure and a change of the adiabatic potential of the tetrahedron. As a result, redistribution of hydrogen/deuterium atoms over their equilibrium positions on the H/D bonds throughout the crystal causes the crystal energy to change. Within the framework of the second-order perturbation theory this change can be determined using the methods of electronic-vibrational (vibronic) theory of heteroligand molecular systems [15–17], considering the fact that each H/D atom is bonded simultaneously to two PO_4 tetrahedrons, specifically, is covalently-bonded to one tetrahedron

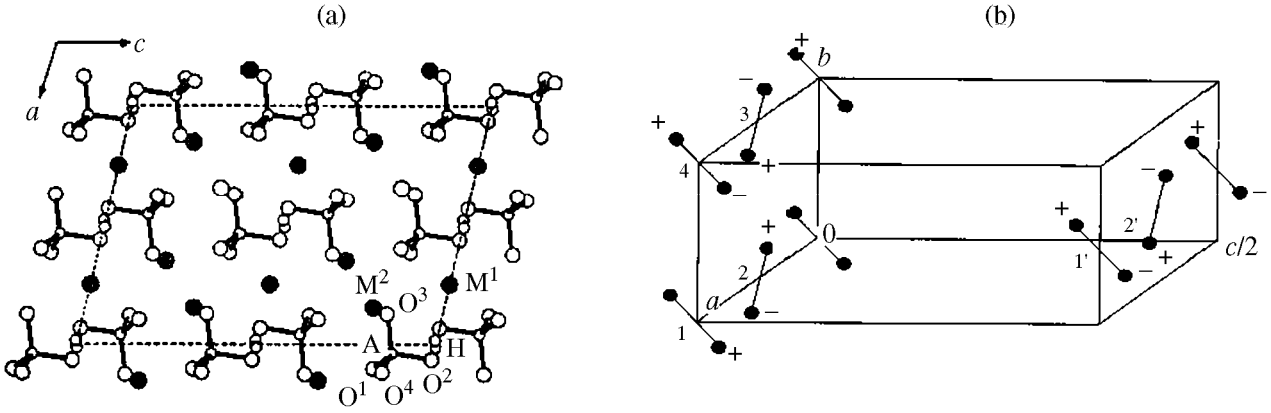

Fig. 5. Structure of TKHS family crystals: (a) projection of the structure onto the (010) plane (two possible sites are displayed for each H atoms); (b) H/D bonds in the unit cell (figures 1, 2, 3, and 4 refer to the nearest neighboring H/D bonds; the "plus" sign corresponds to the covalently-bonded oxygen atom, and "minus" sign, to hydrogen-bonded atom, and the "–"→ "+" vectors show the orientation of the dipoles of the H/D bonds. With only J_{12}, J_{13}, and J_{14} Ising parameters taken into account, the displayed distribution of pseudospins, like all other distributions obtained by their sign reversion in any planes parallel to the ab plane, correspond to the lowest Ising energy.

and hydrogen-bonded to the other. This approach yields [15, 26, 30] the crystal energy in the form (1) in which the automatically produced analytical expressions for the J_{ij} parameters include the characteristics of the molecular-orbital structure of the PO_4 tetrahedron, as well as its vibronic and force constants, which allows deriving the Ising parameters from the calculated results.

The analytical expression for the Ising parameters is also convenient for qualitative analysis of the ferroelectric/antiferroelectric characteristics of the material in relation to its composition and deuteration of H bonds [19].

The TKHS Family

We now turn to application of Hamiltonians (1) and (2) in studying specific materials. First, we will discuss the family of crystals with the composition $M_3H(AO_4)_2$ and their deuterated analogs $M_3D(AO_4)_2$, where M = K, Rb, Cs and A = S, Se (abbr. TKHS family; see Fig. 5a) [31, 32].

Calculations of Ising Parameters

As noted above, the 0-D nature of the H/D bond network allows the J_{ij} parameters for TKHS materials to be calculated in terms of the above-mentioned electrostatic model, using the diffraction data on the geometry of the $(H/D)(AO_4)_2^{3-}$ dimers and their sites in the crystal lattice. To more precisely calculate the Ising parameters, it is more convenient, however, to apply the nonmodel approach [28, 29], which we will term the method of pseudospin (in some cases, simply spin, for brevity) clusters. One version of this method for calculation of the required set of Ising parameters implies singling out one cluster containing the structural units of the crystal, bonded by those H/D bonds, whose interactions correspond to the desired Ising parameters. The total energy of the cluster for all possible distributions of protons over their equilibrium positions on the H/D bonds is expressed in terms of the J_{ij} parameters. Simultaneously, these energies are calculated by some quantum chemical computing procedure, so that the desired J_{ij} parameters can be determined from the resulting system of equations.

We applied this approach in [33] for determining the largest in the absolute value independent Ising parameters J_{12}, J_{13}, and J_{14} corresponding to interaction of protons/deuterons, the nearest and next-nearest neighbors in the crystal (see Fig. 5b). Calculation for the four-spin cluster comprising four $H/D(AO_4)_2$ dimers at 16 possible distributions of protons/deuterons on the H/D bonds was carried out mainly at the RHF level in the 6-311G type bases. For comparison, we used the Moller–Plesset (MP2, MP4) perturbation theory, as well as the inexpensive pseudopotential PP-SBK scheme. As an example we will present the values of the three above-mentioned parameters J_{ij} calculated by the latter method for $K_3H(SO_4)_2$ (98, 22, –36 K) and $K_3D(SO_4)_2$ (156, 36, –55 K)

[33]. They represent these parameters in relation to the mutual separation of the H/D bonds and deuteration of the material. For the same parameters of the six other materials from the TKHS family, see [33].

Calculation of the Tunneling Parameter

The tunneling parameters Ω for the materials examined were calculated using the potential profiles of protons in $[O_3AO–H\cdots OAO_3]^{3-}$ dimers, approximated by the biquadratic function $U(x) = (U_0/a^4)(x^2 - a^2)^2$, where U_0 and $2a$ are the height and width of the proton/deuteron transfer barrier, respectively. In the case discussed, the parameters U_0 and $2a$ were estimated by interpolation based on the results of the RHF and MP2 calculations in the 6-311++(2d, 2p) basic set, since RHF calculations typically overestimate, and MP2 calculations, underestimate the barrier parameters. To calculate these parameters more precisely, the profiles were additionally corrected [33] to take into account the deviations of the proton/deuteron positions, estimated by diffraction methods, from the minima of the double-well potential profile.

The resulting profiles were used for calculating the energy levels of the protons/deuterons by numerically solving one-dimensional Schrödinger equation with the preset potential [34]. Finally, the Ω parameter for each material was calculated as the half-difference of the energies of the two lowest vibrational levels in the double-well adiabatic potential of the hydrogen isotope nucleus. In [33], we presented the tabulated values of the tunneling parameter for eight materials from the TKHS family. Here, we present as an example the rounded Ω values for K3H(SO4)2 and K3D(SO4)2, 430–440 K and 90–100 K, respectively. These data suggest a sharp decrease in Ω upon deuteration of the material due to a greater mass of the deuteron, as well as to an increase in the O···O interatomic distance and the accompanying increase in the distance separating the two equilibrium positions of the heavy hydrogen isotope nucleus (Ubbelohde effect).

Structural Phase Transition to an Ordered Phase

Taking the TKHS family as an example, we will illustrate the application of the parameters of pseudospin Hamiltonians (1) and (2), calculated by quantum chemical methods, in interpreting and predicting the structural and thermodynamic properties of H/D-bonded materials.

Let us consider, above all, application of the Ising model in theoretical calculation of the deuteron positions in an ordered low-temperature phase of completely deuterated crystals from the TKHS family (in nondeuterated samples, no ordered phase is formed, see below). The lack of transfer of deuterons for this phase allows an attempt to accomplish this task using formula (1) and selecting a set of pseudospins σ_i corresponding to the lowest Ising energy. We determined such distributions of pseudospins (see Fig. 5b) in [35]. All of them agree with the experimentally established antiferroelectric nature of the low-temperature phase of the deuterated representatives of the TKHS family. Also, the proposed structures of the deuteron sublattice suggest doubling of the parameter *b* in the paraelectric *A*2/*a* cell of the crystal, associated with a low-temperature transition [36]. The scheme predicted is also consistent with the doubling of the parameter *c*, also noted in [36].

Next, we will apply criterion (4) to the $K_3H(SO_4)_2$ and $K_3D(SO_4)_2$ couple, using the calculated and above-mentioned parameters J_{ij} and Ω and taking into account $J_0 = {}^2J_{12} + {}^4J_{13} + {}^2J_{14}$ for this case. Hence, a struc-tural transition to the ordered phase should be observed in the latter compound characterized by $\Omega/J_0 < 1$.

Figure 5b shows that this is an antiferroelectric phase. At the same time, no transition to the ordered phase should occur in the former compound, for which $\Omega/J_0 > 1$ holds. A similar situation is observed for other H/D couples of materials from the TKHS family [33]. This is consistent with the experimental data [32] and is associated with the fact that, in the materials examined, the quantum fluctuations of protons, by contrast to deuterons, are too large and result in preservation of the disordered, paraelectric state at all temperatures (the so-called quantum paraelectric behavior). It should be noted, however, that, according to the calorimetric data [32], the $K_3H(SeO_4)_2$ crystal still exhibits a phase transition at ~20 K. However, its interrelation with the proton subsystem ordering still remains to be elucidated more precisely.

Crystalline Derivatives of Hydroxyphenalenone

Organic molecules that can exist as two possible tautomeric forms seem to be suitable as structural units for ferro- and antiferroelectric materials. This idea was successfully implemented [37, 38] through synthesis of a new family of 0-D materials with intramolecular H/D bonds, 5X derivatives of 9-hydroxyphenalenone (abbr. 5X-9HPO) and its deuterated analog (Fig. 6), where X =

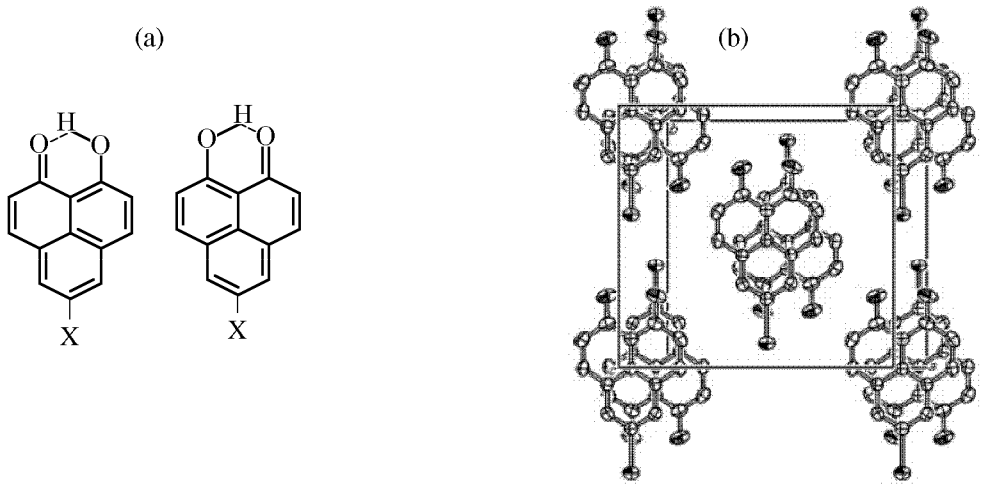

Fig. 6. (a) Tautomeric forms of the molecule and (b) structure of the crystal (as viewed from the c axis, with hydrogen atoms not displayed) for 5X derivatives of 9-hydroxyphenalenone [41].

Br [39, 40], I [41, 42], and CH_3 [37, 38]. Experiments showed that, similar to $M_3H(AO_4)_2$ materials, both halogenated 9HPO compounds exhibit a low-temperature quantum paraelectric behavior down to 4 K. At the same time, 5Br–9DPO and, possibly, 5I-9DPO pass to an ordered phase at temperatures below 20 and 25 K, respectively. Such extremal thermodynamic H/D isotope effect is not characteristic for $5CH_3$-9(H/D)PO compounds in which a low-temperature ordered antiferroelectric state is observed at temperatures below 40 K both for the protonated and deuterated forms. For brevity, we will restrict ourselves to discussion of halogenated 9(H/D)PO compounds [43, 44] (for the CH_3 derivative, see [43]).

Parameters of the Pseudospin Hamiltonian

To interpret the temperature dependence of the phase state of the crystalline derivatives of 9(H/D)PO compounds, we calculated the parameters Ω and J_{ij}. The tunneling parameters Ω were determined by interpolation of the data of RHF/3-21G and B3LYP/6-311G(2d,2p) calculations for an isolated 9-hydroxyphenalenone molecule. The potential barrier of the proton transfer was calculated by the transition state method using the QST2 procedure from the GAUSSIAN-98 package; the geometric parameters of the molecules of the "reactants" and "products" were calculated at the RHF and DFT levels by full optimization of the enolic forms of the molecule in the ground electronic state. In view of identity of the O···O distances (lacking Ubbelohde effect) the potential profiles of the proton and deuteron were taken as identical. Like in the case of the TKHS family, the one-dimensional Schrödinger equation was solved using the biquadratic approximation of the adiabatic potential of the proton and the numerical method [34].

To determine the five independent Ising parameters corresponding to the interaction between the H bonds of the 5X-9HPO molecules both in the same and in the neighboring piles of molecules (see Fig. 6), we carried out RHF and B3LYP calculations for five two-spin clusters, to which end formula (5) was applied five times. The $V_{ij}(+, -)$ etc. terms in formula (5) stood for total energies of the clusters, each comprising two 5X-9HPO molecules at different possible distributions of two protons over their equilibrium positions on the H-bonds. Because of incomplete information about the crystal structure of the 9-hydroxyphenalenone derivatives the J_{ij} parameters were calculated for slightly idealized packing of the molecules in the 5I-9HPO crystal. To simplify the calculations, the Br and I substituents in the hydroxyphenalenone molecule were simulated by H atoms, which, in particular, enables the use of the basis sets enlarged relative to the minimal 3-21G basis.

The resultant Ω(H) and Ω(D) parameters for brominated and iodinated 9-(H/D)PO compounds were estimated at ca. 75 and 12 K, respectively (by interpolation of the barrier parameters between the corresponding RHF and B3LYP data). At the same time, the J_0(H) and J_0(D) parameters determined by

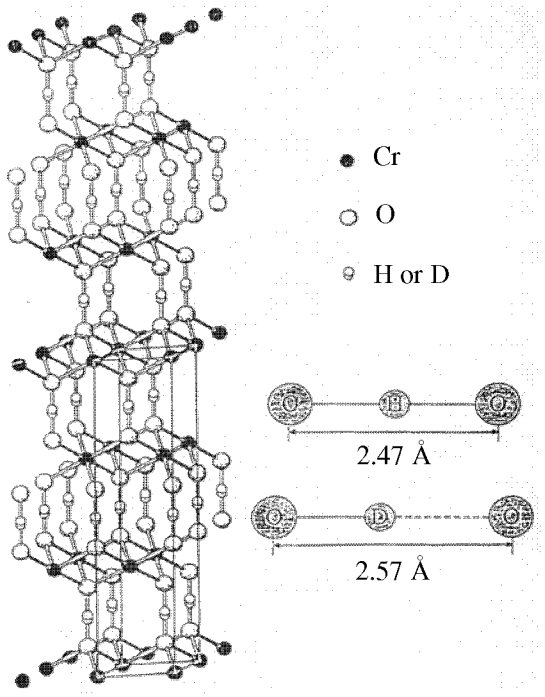

Fig. 7. Crystal structure of α-$HCrO_2$ and α-$DCrO_2$ [46].

similar interpolation of the Ising parameters are identical, ca. 30 K, for the two halogenated compounds of interest (because of the lacking Ubbelohde effect).

Phase States of 5X-9(H/D)PO Compounds

The tunneling and molecular field parameters we determined cannot be substituted in the left parts of inequalities (4) without certain reservations, since, strictly speaking, the molecular field approximation is inapplicable in this case, because the 5Br-9HPO and, possibly, 5I-9HPO compounds contain a narrow band of noncommensurable phases separating the paraphase from the ordinary (commensurable) ordered phase [39, 40]. However, physically it is obvious that the phase state of the H/D-bonded material is determined by competition of the ordering effect of the cooperative bond of the protons/deuterons (described by the J_0 parameter) and the disordering effect of the quantum motion of these nuclei (described by the parameter Ω). Therefore, a large Ω/J_0 ratio of 2.6 for the 5X-9HPO compounds suggests that the disordered paraelectric phase can be preserved down to the lowest temperatures, as is really the case. A fairly small W/J_0 ratio of 0.4, by contrast, suggests the existence of a low-temperature ordered phase in the 5X-9DPO derivatives, as experimentally established for compounds with X = Br and not ruled out for X = I.

Calculations by formula (1) of the Ising energy of the crystalline halogenated 5X-9DPO compounds predict that, like in the case of the TKHS family, a lower energy will be exhibited by antiferroelectric low-temperature ordered state of the deuterons (at which the dipoles of the D-bonds of the neighboring molecules in each pile of molecules and throughout the crystal lattice are oppositely oriented), rather than by the ferroelectric state. Such ordering seems natural from the electrostatic viewpoint, since for the 0-D crystals of the 9-hydroxyphenalenone derivatives the electrostatic model of the proton/deuteron bonds seems fairly adequate. We will note that, in a similar case of $5CH_3$–9(H/D)PO crystals, the ordered phase is also of the antiferroelectric type [43].

Crystalline α-Chromous Acid

One more example of application of quantum chemistry approaches in studies of H-bonded materials in the framework of Hamiltonians (1) and (2) can be found (like in [47]) in the crystalline α-modification of chromous acid $HCrO_2$ and its deuterated analog $DCrO_2$ (Fig. 7), whose specific properties were noted by Matsuo et al. [40, 45, 46]. Both forms exhibit a magnetic phase transition at close temperatures (22 and 25 K), while only the latter occurs in a (deuteron-) ordered phase below an unusually high temperature T_c = 320 K. The protonated form of α-$HCrO_2$ exhibits no order–disorder structural phase transition.

Another feature specific of α-chromous acid is a uniquely large Ubbelohde effect: According to the neutron diffraction data [46], upon deuteration of the H-bonds the O···O distance increases by 0.1 Å (for the TKHS family, this effect does not exceed 0.04 Å).

Modeling of the Structure of α-(H/D)CrO_2

Modeling of the structure of α-chromous acid is a fairly difficult task, as any realistic Cr-containing cluster should comprise a fairly large number of metal atoms. In interpreting the influence of deuteration on the properties of this material, the situation can be simplified by taking into account the role (probably, deciding) played by the huge Ubbelohde effect and replace the real structure of the crystal by the system of its H/D-bonds (although this means neglecting the mechanism of indirect nonelectrostatic interaction of protons/deuterons). An attempt to reproduce the characteristic features of the layered system of the H/

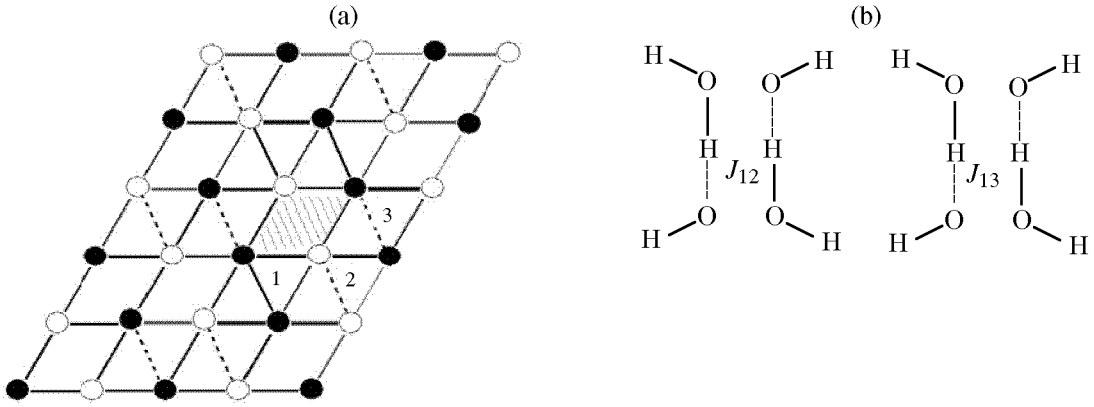

Fig. 8. To calculation of Ising parameters for α-chromous acid: (a) schematic representation of the "oxygen" plane in α-$HCrO_2$ and α-$DCrO_2$ crystals (open circles designate the $O_{O–H}$/D atoms, and solid circles, $O_O\cdots_H$/D atoms) and (b) two two-spin clusters in which the H/D bonds are modeled by $H_3O_2^-$ molecular groups.

D-bonds in the crystal can be realized, in turn, with a layer composed of the model $[HO–H/D\cdots OH]^-$ or $[H_2O–H/D\cdots OH_2]^+$ molecules in which the geometry of the H/D-bonds (with "manually" set lengths, orientations, relative positions, and spacings) is identical to that in real α-(H/D)CrO_2 crystals.

Calculations of the Tunneling Parameters

Such (preliminary) modeling of the system of H/D-bonds in α-chromous acids, incidentally based on incomplete structural information, requires increasing the volume and level of the calculation to decrease the artefacts in the final conclusions. The calculations in [47] utilized a number of nonempirical schemes, from RHF and B3LYP to MP4 and coupled cluster methods CCSD and CCSD(T) primarily in the 6-311G, 6-311++G, and cc-pvtz bases. The calculations were carried out for different O···O distances from the 2.40–2.80 Å range for linear hydrogen bonds in the model $H_3O_2^-$ and $H_5O_2^+$ species. For the terminal OH and OH_2 groups in the $H_5O_2^+$ species we also considered different versions corresponding both to the fixed geometry of groups and the optimized geometry. We gave special attention to calculations at the experimental O···O distances of 2.47 Å in α-$HCrO_2$ and 2.57 Å in α-$DCrO_2$. This yielded the ranges of the most acceptable values of the transfer barrier parameters for the hydrogen isotopes: $0.2 < U_0 < 1.2$ kcal mol^{-1}, $0.25 < 2a < 0.33$ Å for α-$HCrO_2$ (2.47 Å), and $1.4 < U_0 < 3.7$ kcal mol^{-1}, and $0.43 < 2a < 0.49$ Å for α-$DCrO_2$ (2.57 Å), where U_0 and 2a are the barrier height and width, respectively. However, in reality, we considered slightly wider ranges for the U_0 and $2a$ parameters, which yield, eventually, the corrected Ω values varying within $350 < \Omega(H) < 780$ K and $30 < \Omega(D) < 170$ K.

Calculation of Ising Parameters

Following the adopted (layered) structural model of the H/D-bonds in α-(H/D)CrO_2 crystals, Fig. 8a shows the structure of either of the two "oxygen" planes belonging to the chosen layer, e.g., of the bottom plane from which the relative positions of these bonds in this layer can be easily seen. The J_{ij} parameters for this layer were calculated in the two-spin cluster approximation (Fig. 8b), taking into account pseudospins, the nearest and next-nearest neighbors designated in Fig. 8a as 1,2 and 1,3, respectively. Every term in formula (5) was estimated using nine different computing schemes, from B3LYP and RHF to CCSD(T) in the 6-311G and 6-311G++ bases. The resulting value of the molecular field parameters J_0 for α-$HCrO_2$ varies from ~150 to 230 K, depending on the type of calculation, and that for α-$DCrO_2$, from 670 to 980 K.

Structural Phase Transition

The above-presented data on the molecular-field and tunneling parameters for α-chromous acid suggest that, at any combination of the acceptable numerical values of the Ω(D) and J_0(D) parameters, the Ω/J_0 ratio is always less than unity (even less than 0.25). At the same time, for an arbitrary combination of the acceptable parameters Ω(H), J_0(H), the Ω/J_0 ratio is over unity, more precisely, more than 1.5. According to criterion (4), this means that the deuterated α-chromous acid should necessarily undergo a structural transition to a deuteron-ordered phase, whereas

nondeuterated samples of this material should exhibit a quantum paraelectric behavior, which is fully consistent with the experiment [40, 45, 46].

Role of the Ubbelohde Effect

A more detailed analysis [47] shows that the observed deuteration-induced structural phase transition is closely connected to the huge Ubbelohde effect, lengthening of the O–D···O bond to 2.57 Å. However, inequality (4a) also holds at smaller lengths of this bond, in particular, at the O···O distance of 2.53 α, identified as the lower limit of the possible length of the O–D···O bond in α-$DCrO_2$ crystals [48, 49].

The Ubbelohde effect is also responsible for a fairly high critical temperature of the phase transition (320 K) which was theoretically estimated by us using the Bethe's "cluster method." This method is widely used in statistical physics of cooperative phenomena [50]; it was first applied to an H-bonded material (KH_2PO_4) in [51].

In the Bethe's method, the coupling of individual pseudospins inside an isolated group of pseudospins is accurately taken into account in terms of the Ising model, and the coupling of the pseudosipns of this group with external pseudospins of the crystal lattice are considered in terms of the mean field approximation. We applied this approach within the framework of the method of two-spin cluster (see Fig. 8b) and a more complex four-spin cluster; in both cases we took 2.53 Å for the O–D···O bond length and 1.07 Å, calculated by the CCSD(T) method, for the O–D bond length (its experimental value is unknown). This yielded T_c of 400 K (two-spin clusters) and 330 K (four-spin cluster), which is fairly close to the measured value of 320 K.

Lastly, we will mention the predicted type of deuteron ordering in α-$DCrO_2$ at temperatures below T_c. In terms of the single-layered model of the H/D-bond system, we utilized for α-chromous acids, it would be natural to expect antiferroelectric, rather than ferroelectric, positions of the deuterons, at which the dipole corresponding to each D-bond is surrounded by the maximal number of antiparallel dipoles, as shown in Fig. 8a. This type of antiferroelectric ordering is energetically preferable, as confirmed by Ising energy calculations (1).

ACKNOWLEDGMENTS

This study was financially supported by the Russian Foundation for Basic Research (project no. 05-03-32648) and a grant of the Department of Chemistry and Materials Science, Russian Academy of Sciences, Program 1.

REFERENCES

1. Lines, M.E. and Glass, A.M., *Principles and Applications of Ferroelectrics and Related Materials*, Clarendon: Oxford, 1977.
2. Blistanov, A.A., *Kristally kvantovoi i nelineinoi optiki* (Quantum and Nonlinear Optics Crystals), Moscow: Mosk. Inst. Stali Splav., 2007.
3. Baranov, A.I., *Kristallografiya*, 2003, vol. 48, p. 1081.
4. Korby, T., *Nature*, 2001, vol. 410, p. 877.
5. Halle, S.M., Boysen, D.A., et al, *Nature*, 2001, vol. 410, p. 910.
6. Sonin, A.S., in *Segnetoelektriki* (Ferroelectrics), Rostov. Univ., 1968, p. 5.
7. Levin, A.A., Fedorova, I.S., and Zaitsev, A.R., *Zh. Neorg. Khim*., 1988, vol. 33, p. 62.
8. Levin, A.A., Zaitsev, A.R., and Isaev, A.N., *Zh. Neorg. Khim*., 1989, vol. 34, p. 2418.
9. Burshtein, K.Ya. and Isaev, A.N., *Theor. Chim. Acta,* 1984, vol. 64, p. 397.
10. Bystrov, D.S. and Popova, E.A., *Fiz. Tverd. Tela,* 1981, vol. 23, p. 1461.
11. Nelmes, R.T., *Ferroelectrics*, 1987, vol. 71, p. 125.
12. Levin, A.A. and Dolin, S.P., *Dokl. Ross. Akad.* Nauk, 1996, vol. 351, no. 4, p. 502.
13. Levin, A.A., Dolin, S.P., and Lebedev, V.L., *Zh. Neorg. Khim.*, 1997, vol. 42, p. 1321.
14. Boys, S.F., in *Quantum Theory of Atoms, Molecules, and Solid State*, Löwdin, P.O., Ed., New York: Interscience, 1967, p. 253.
15. Levin, A.A. and Dolin, S.P., *Koord. Khim*., 1998, vol. 24, p. 287.
16. Levin, A.A., *Koord. Khim*., 1993, vol. 19, p. 368.
17. Levin, A.A. and D'yachkov, P.N., *Heteroligand Molecular Systems: Bonding, Shapes, and Isomer Stabilities*, London: Taylor&Francis, 2002.
18. Lebedev, V.L., Dolin, S.P., and Levin, A.A., *Zh. Neorg. Khim.*, 1995, vol. 40, p. 1683.
19. Levin, A.A., Dolin, S.P., and Lebedev, V.L., *Khim. Fiz*., 1995, vol. 14, no. 9, p. 84.
20. Schmidt, V.H., Wang, J.T., and Schackenberg, W., *Jpn. J. Appl. Phys*., 1985, vol. 24, suppl. 24-2, p. 944.
21. Matsushita, E. and Matsubara, T., J. *Phys. Soc. Jpn.,* 1987, vol. 56, no. 1, p. 200.
22. Vaks, V.G., *Vvedenie v mikroskopicheskuyu teoriyu segnetoelektrikov* (Introduction to Microscopic Theory of Ferroelectrics), Moscow: Nauka, 1973.

23. Vaks, V.G., Zinenko, V.I., and Shneider, V.E., *Usp. Fiz. Nauk*, 1983, vol. 141, p. 629.
24. Moritomo, Y., Tokura, Y., Nagaosa, N., Suzuki, T., and Kumagai, K., *Phys. Rev. Lett.*, 1993, vol. 71, p. 2833.
25. de Gennes, P.G., *Solid State Commun*., 1963, vol. 1, no. 6, p. 132.
26. Levin, A.A. and Dolin, S.P., *J. Mol. Struct*., 2000, vol. 552, p. 39.
27. Levin, A.A., Dolin, S.P., Mikhailova, T.Yu., and Kirillova, N.I., *J. Mol. Liquids*, 2003, vol. 106, nos. 2–3, p. 223.
28. Dolin, S.P., Levin, A.A., Solin, M.V., Borisov, E.V., and Strokach, N.S., *Khim. Fiz.*, 2002, vol. 21, no. 2, p. 94.
29. Dolin, S.P., Levin, A.A., Mikhailova T.Yu, Solin, M.V., and Trakhtenberg, L.I., *Int. J. Quant. Chem.*, 2002, vol. 88, p. 463.
30. Levin, A.A. and Dolin, S.P., *J. Phys. Chem.*, 1996, vol. 100, p. 6258.
31. Ichikawa, M. and Matsuo, T., *J. Mol. Struct*., 1996, vol. 378, p. 17.
32. Onoda-Yamamuro, N., Yamamuro, O., et al., *J. Phys.: Cond. Matt.*, 2000, vol. 12, p. 8559.
33. Dolin, S.P., Levin, A.A., Mikhailova, T.Yu, et al., *Int. J. Quant. Chem.*, 2004, vol. 96, p. 247.
34. Mikhailova, T.Yu. and Pupyshev, V.I., *Opt. Spektr.,* 1999, vol. 87, p. 35.
35. Dolin, S.P., Levin, A.A., Mikhailova, T.Yu., and Solin, M.V., *Adv. Quant. Chem*., 2003, vol. 44, p. 579.
36. Tamura, I. and Noda, Y., *Ferroelectrics*, 1998, vol. 219, p. 135.
37. Sugawara, T., *J. Crystallogr. Soc. Jpn*., 1994, vol. 36, no. 6, p. 12.
38. Mochida, T., Izuoka, A., Sugawara, T., Moritomo, Y., and Tokura, Y., *J. Chem. Phys*, 1994, vol. 101, p. 7971.
39. Tamura, I., Noda, Y., Kuroiwa, Y., Mochida, T., and Sugawara, T., *J. Phys.: Cond. Matter,* 2000, vol. 12, p. 8345.
40. Matsuo, T., *Pure Appl. Chem*., 2003, vol. 75, p. 913.
41. Mochida, T., Suzuki, S., Takasu, I., and Sugawara, T., *J. Phys. Chem. Solids*, 2003, vol. 64, p. 1257.
42. Matsuo, T., Baluja, S., Koike, Y., Ohama, M., Mochida, T., and Sugawara, T., *Chem. Phys. Lett*., 2001, vol. 342, p. 22.
43. Dolin, S.P., Levin, A.A., Polyakov, E.V., Khrulev, A.A., and Mikhailova, T.Yu., *J. Mol. Struct*., 2006, vol. 790, p. 147.
44. Dolin, S.P., Khrulev, A.A., Polyakov, E.V., Mikhailova, T.Yu., and Levin, A.A., *Int. J. Quant. Chem.,* 2006, vol. 106, p. 2297.
45. Matsuo, T., Inaba, A., Yamamuro, O., and Onoda-Yamamuro, N., *J. Phys.: Cond. Matter,* 2000, vol. 12, p. 8595.
46. Matsuo, T., Maekava, T., Inaba, A., et al., *J. Mol. Struct.*, 2006, vol. 790, p. 129.
47. Dolin, S.P., Flyagina, I.S., Tremasova, M.V., et al., *Int. J. Quant. Chem*., 2007, vol. 107, p. 2409.
48. Ichikawa, M., Gustafsson, T., Olovsson, I., and Tsuchida, T., *J. Phys. Chem. Solids*, 1999, vol. 60, p. 1875.
49. Ichikawa, M., *J. Mol. Struct*., 2000, vol. 552, p. 63.
50. Kubo, R., *Statistical Mechanics*, Amsterdam: North-Holland, 1965.
51. Blinc, R. and Svetina, S., *Phys. Rev*., 1966, vol. 147, no. 2, p. 430.